Experimental investigation of augmented thermal and performance characteristics of solar air heater ducts due to varied orientations of roughness geometry on the absorber plate

MUKESH KUMAR SAHU[a*]
M.M. MATHESWARAN[b]
PARDEEP BISHNOI[c]

[a] Department of Mechanical Engineering, National Institute of Technology, Jamshedpur Jharkhand, Pin-831014, India

[b] Department of Mechanical Engineering, Jansons Institute of Technology, Karumathampatti, Coimbatore, Tamil Nadu, 641659, India

[c] Department of Mechanical Engineering, Chandigarh Engineering College, Mohali, Punjab, 140307, India

Abstract   This paper presents the outdoor experimental results for thermal performance analysis of artificially roughened solar air heaters (SAHs). Circular wire ribs have been arranged to form arc shape geometry on the absorber plates and have been tested for two configurations of SAHs named as arc shape apex-downstream flow and arc shape apex-upstream flow SAH. Roughness parameters have been taken as relative roughness pitch in the range of 8–15, angle of attack 45°–75°, and for fixed relative roughness height of 0.0454, duct width to duct height ratio of 11. During the experimental analysis the mass flow rate varied from 0.0100 to 0.0471 kg/s. Based on the experimental results it was found that roughness with apex-upstream flow SAH is having higher value of thermal efficiency, heat removal factor and collector efficiency factor as compared to roughness with apex-downstream flow SAH and simple absorber plate SAH. In the range of the operating parameters investigated the maximum of thermal efficiency, heat removal factor, and collector efficiency factor have been found.

Keywords: Solar air heaters (SAHs); Thermal efficiency; Heat removal factor; Collector efficiency factor; Artificial roughness; Heat transfer rate

*Corresponding Author. Email: mks.nitjsr@gmail.com

Nomenclature

A_c	–	surface area of absorber plate, m^2
A_o	–	area of orifice of orifice plate, m^2
C_{pa}	–	specific heat of air, J/kg
C_d	–	coefficient of discharge for orifice meter
D	–	hydraulic diameter of duct, m
E	–	roughness height, m
g	–	acceleration due to gravity, m/s^2
G	–	mass flow rate of air per unit collector area, kg/s m^2
h	–	heat transfer coefficient, $\text{W/m}^2\text{K}$
h_w	–	convective heat transfer coefficient due to wind, $\text{W/m}^2\text{K}$
H	–	depth or height of solar air heater duct, m
I	–	intensity of global solar radiation (insolation), W/m^2
K_a	–	thermal conductivity of air, W/m K
K_g	–	thermal conductivity of glass cover, W/m K
K_i	–	thermal conductivity of glass wool insulation, W/m K
L	–	length of solar air heater duct, m
L_1	–	spacing between glass cover and absorber plate,m
L_g	–	thickness of glass cover, m
$\dot{M}$	–	mass velocity of air, kg/s m^2
Ng	–	number of glass covers
$\dot{m}$	–	mass flow rate of air, kg/s
ΔP	–	pressure drop across the collector duct, N/m^2
ΔP_D	–	pressure drop across test section, N/m^2
ΔP_o	–	pressure drop across orifice meter, N/m^2
P	–	roughness pitch, m
P_m	–	pumping power, W
p_a	–	atmospheric pressure, N/m^2
Q_u	–	useful heat gain, W
ΔT	–	rise in air temperature, $^\circ$C
T_{sun}	–	sun temperature, K
$\Delta T/I$	–	temperature rise parameter, $^\circ$C m^2/W
T_g	–	cover glass temperature, K
T_{fo}	–	outlet air temperature, K
T_s	–	sky temperature, K
T_{fi}	–	air inlet temperature, K
T_a	–	ambient temperature, K
T_{pm}	–	mean absorber plate temperature, K
T_{fm}	–	mean air temperature in the duct, K
T_{bm}	–	mean temperature of bottom plate, K
U_L	–	overall heat loss coefficient, $\text{W/m}^2\text{K}$
U_b	–	bottom loss coefficient, $\text{W/m}^2\text{K}$
U_s	–	side loss coefficient, $\text{W/m}^2\text{K}$
U_t	–	top loss coefficient, $\text{W/m}^2\text{K}$
V	–	average velocity of air through the duct, m/s
V_w	–	wind velocity, m/s
W	–	width of solar air heater duct, m
$\dot{W}_p$	–	pumping or mechanical power, W

Dimensionless parameters

d/w	–	relative gap position
e/D	–	relative roughness height
f	–	friction factor
F_R	–	collector heat-removal factor
F'	–	collector efficiency factor
F_o	–	collector heat removal factor referred to outlet air temperature
G'	–	heat transfer function
Nu	–	Nusselt number
P/e	–	relative roughness pitch
Pr	–	Prandtl number
R	–	roughness function
Ra	–	Rayleigh number
Re	–	Reynolds number
Re^+	–	roughness Reynolds number
St	–	Stanton number
W/w	–	relative roughness width
W/H	–	aspect ratio of collector duct
$1r$	–	one side roughness
$3r$	–	three sides roughness

Greek symbols

μ	–	absolute viscosity of air, Ns/m^2
ρ	–	air density, kg/m^3
α	–	angle of attack, degree
σ	–	Stefan-Boltzman constant, $\text{W/m}^2\ \text{K}^4$
δ_i	–	insulation thickness, m
β	–	tilt angle of collector surface, degree
ν	–	kinematic viscosity of air, m^2/s
η_{th}	–	thermal efficiency
$(\tau\alpha_p)_e$	–	effective transmittance-absorptance product
$\alpha/90$	–	relative angle of attack
α_c	–	absorptivity of the glass cover
ε_p	–	emissivity of absorber plate
ε_b	–	emissivity of bottom plate
ε_g	–	emissivity of glass cover
α_p	–	absorptivity of absorber plate
β_R	–	ratio of orifice diameter (D_2) to pipe internal diameter (D_1)
τ	–	transmissivity of glass cover

1   Introduction

Among all the available free non-conventional energy sources, solar energy
is the source of energy which is freely available on the earth's surface. Solar
energy reached on the earth surfaces in the form of solar radiations which is

utilized for the various mankind and industrial applications by converting this into other useful forms of energy, i.e., thermal energy through using various solar thermal systems. Flat plate solar collectors (SC) i.e. solar water heaters (SWH) and solar air heaters (SAH) are the majorly used as solar thermal energy conversion systems. Different thermal energy conversion systems are found to be lower thermal efficiencies due to poor heat transfer rate or interaction between the heated surfaces and flowing fluids. Several researchers have made their efforts towards enhancing the heat transfer rate in SAH duct by using different methods.

Prasad and Saini firstly who studied the effect and application of thin circular wires as artificial roughness in the form of different roughness parameters, i.e., relative roughness height (e/D) and relative roughness pitch (P/e) with the arrangement of roughness geometry named as 'transverse' in the rectangular duct of SAH [1]. They reported maximum enhancement in the Nusselt number as 2.38 times and on the friction factor as 4.25 times with respect to the smooth absorber plate SAH. After that, several authors have used artificial roughness (with thin circular diameter wires) in the absorber plate with different arrangement of wires to form roughness geometries like Gupta *et al.* [2] investigated continuous inclined; Aharwal *et al.* [3] investigated continuous inclined with gap, Momin *et al.* [4] investigated continuous V-shape, ribs, Hans *et al.* [5] investigated multiple V-shape wire roughness geometry. Kumar *et al.* [6] investigated experimentally the effect of the gap in multiple V-shape ribs, Lanjewar *et al.* [7] performed an experimental investigation for discrete W-shaped wire rib geometry.

Lanjewar *et al.* [8] explored the effect on heat transfer and friction factor of a SAH for different orientations of W-shaped roughness geometry, i.e., W-up and W-down. Singh *et al.* [9] carried out experimental investigations for multiple arc-shape wire rib roughness geometry.

An experimental investigation has been carried out by Pandey *et al.* [10] to analyze the effect of the multiple arc-shaped roughness with gaps on heat transfer and friction factor of a SAH. Hans *et al.* [11] carried out an experimental investigation to study the effect of broken arc rib roughness on thermal and frictional characteristics of SAH duct. Gill *et al.* [12] carried out the study of SAH roughened by broken arc ribs combined with a staggered rib piece. All authors have used wire ribs as roughness element, its geometries on the absorber plate in order to perform their experimental investigations. On the basis of their experimental data they have also developed the correlations for heat transfer in terms of the Nusselt number

(Nu) and friction characteristics. These correlations are used to predict the performance of those SAHs under various roughness parameters and operating conditions and will help to design an optimal solar air heater. Saini and Saini experimentally studied the effect of relative roughness pitch (p/e), relative roughness height (e/D) and relative arc angle ($\alpha/90$) for the circular wire ribs in arc shape geometry [13]. Various performance analysis and optimization [14–17] have been carried out for the arc shape by using the developed correlations given by [13].

From the literature survey, it was found that few performance investigation have been performed in actual outdoor conditions for roughened SAHs. Although various modifications have been introduced like creating gaps, combining staggered pieces with gap, etc. little have been carried out for arc shape wire rib roughness [9–12]. It is reported that different shapes of roughness elements and orientations of roughness elements also affect the heat transfer and friction factor significantly [18, 19].

As per author's best knowledge, no detail work has been carried out in order to investigate the effect of different orientation, i.e., apex-downstream and apex-upstream flow of arc shaped wire ribs on thermal performance, heat transfer, friction factor and pressure drop of a SAH duct.

In present work an experimental investigation has been carried out with an aim to investigate the thermal performance enhancement of SAHs using commercially available galvanized iron (GI) wires of circular in shape of parallel arcs as artificial roughness with (i) apex-upstream and (ii) apex-downstream on the air flow side of the absorber plate by [20]. The experiments have been conducted in actual outdoor conditions for the specified values/range of operating system and roughness parameters. The experimental results of [20] have been presented in this paper.

The thermal efficiencies of the solar air heaters with the above mentioned two geometries of the wire-roughness have been evaluated using the experimental data and their comparative performances have been studied and reported in this article. Table 1a shows the comparison of different roughness and operating parameters between present investigation and research have been carried out by Saini and Saini for arc shape roughness [13].

2   Details of experimental setup

The experimental setup has been designed and fabricated as per the ASHRAE standards for operation of the solar air heaters in an open loop

system [21]. The complete setup was installed on the roof of Mechanical Engineering Department at National Institute of Technology, Jamshedpur (India) which is at a geographical location of 22°48′ N, and 86°11′ E. Figure 1 shows the photograph of experimental setup which consists of wooden rectangular duct with entry, test and exit sections and GI pipe equipped with discharge measuring instruments each for the roughened and smooth absorber plate SAHs. A 5 HP Centrifugal blower with a 3.5 kW electric motor has been provided in the setup to suck air from the atmosphere through the test sections.
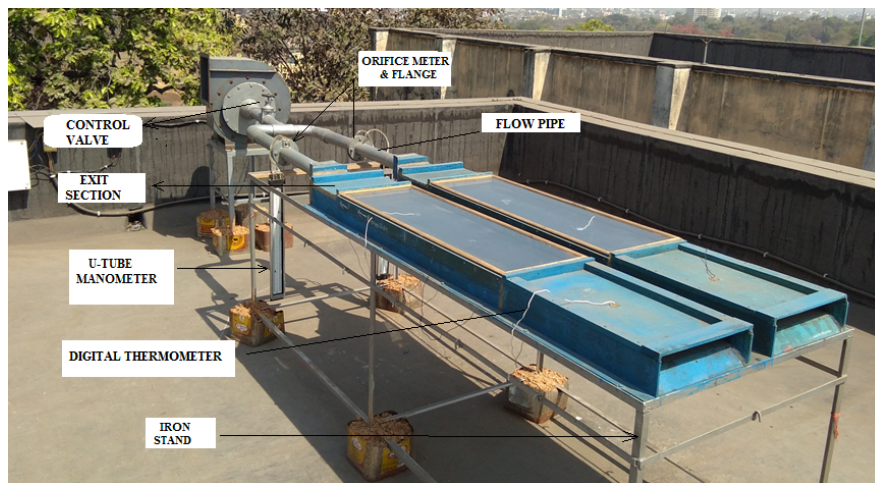
Figure 1: Photograph of experimental setup.

The rectangular duct is having dimensions of 2150 mm × 330 mm × 30 mm in which the length of the test section is 1200 mm and lengths of entry and exit sections are 650 mm and 300 mm, respectively. The test section of one of the ducts consists of the roughened absorber plate while the parallel test section consists of a smooth absorber plate. The aspect ratio, the width to the height (W/H), of the duct is 11.

It may be noted that the minimum lengths of entry and exit sections of the duct are taken equal to $5\sqrt{(WH)}$ and $2.5\sqrt{(WH)}$ respectively for the turbulent flow of air in the duct as per ASHRAE standard 93–77, consequently, the flow can be assumed to be fully developed turbulent in the entire length of the test section. Exit section is required to provide with the test section to minimize the end effects in the test section. The entry section is made with a bell-mouth shape at the inlet side to avoid loses

at the entry. The bottom and sides of the duct are made of good quality wooden plywood of 19 mm thickness. Each test section contains a glass cover of 4 mm thickness at the top and a back plate of 3 mm thick GI sheet in the bottom. The absorber plate, back plate and two wooden side walls form the duct through which air is made to flow.

Glass wool insulation of 50 mm thickness has been used between the back plate and plywood to prevent loss of heat through the bottom. A control valve was provided to control the flow in both the ducts. Figure 1 shows the photograph of the facility whereas its details are shown in Fig. 2.
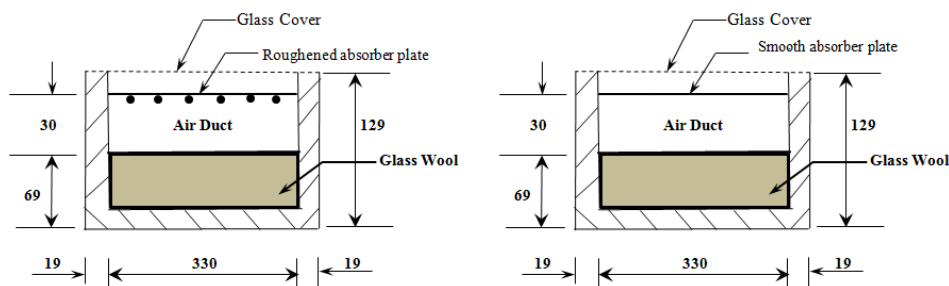
Figure 2: Test sections for roughened and smooth plate solar air heaters (all dimensions are in mm).

2.1   Instrumentation

2.1.1   Measurement of mass flow rate of air across the test section

The mass flow rate of air was measured by means of a calibrated orifice meter connected to the GI pipe. The orifice plate and flange taps have been designed and fabricated according to specifications given in reference [18] for a pipe diameter of 66 mm outside diameter (OD). The orifice plate is so adjusted between the flanges of the pipe that the plate holes remain concentric with the pipe. The U-tube manometer is connected to the pressure taps fixed at a distance of 25 mm upstream and downstream of the orifice plate.

The manometric reading (Δh) was recorded with a U-tube manometer (of 300 mm scale with water as a manometric fluid) fitted across the orifice meter. This value of (Δh) was used to calculate the pressure drop (ΔP_o) and finally the mass flow rate of air $(\dot{m})$ through the test section. Figure 3a shows the details of orifice plate and flange.
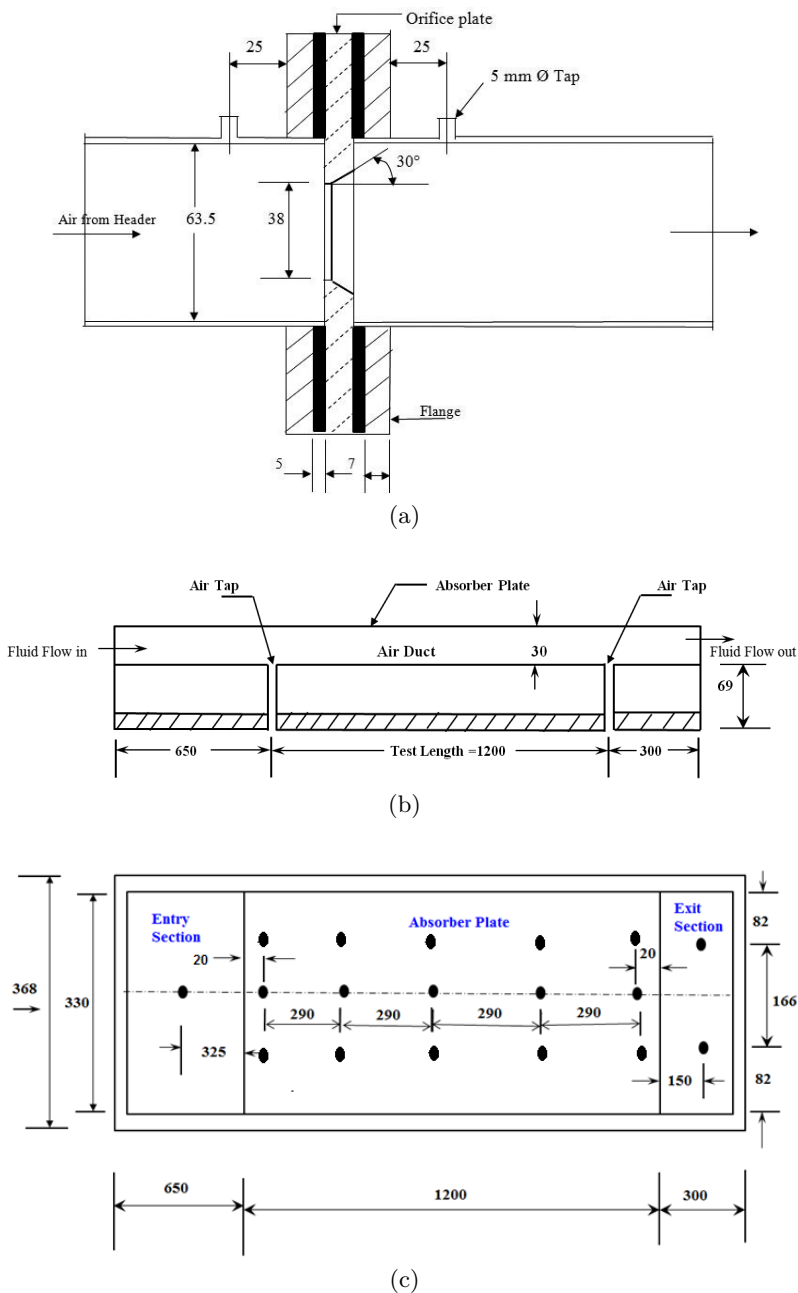
(a)

(b)

(c)

Figure 3: a) Orifice meter and flange construction. b) Location of pressure taps in the test-section of SAH duct. c) Locations of digital thermocouples on entry and exit sections and on absorber plate. All dimensions are in millimeters.

2.1.2   Measurement of pressure drop of air across the test section

The pressure drop across the test section (ΔP_D) was measured with the help of a U-tube micromanometer having least count of 0.01 mm of water column. To measure the static pressure, drop across the test section, two pressure taps, each of 6 mm diameter, have been provided at the bottom side of the duct, along the length of the test sections. Location of pressure taps along the length of the test section is shown in Fig. 3b. This value of pressure drop was used to measure the friction factor (f) and the pumping power expended in the duct during the flow of air through it.

2.1.3   Measurement of absorber plate and air temperatures across the test section

Digital thermocouples were used to measure the air temperature at inlet and outlet of the test section and absorber plate temperatures at various locations, as shown in Fig. 3c, for both test sections.

2.1.4   Measurement of intensity of solar radiation

The intensity of solar radiation (insolation) on horizontal surface was measured with the help of a digital pyranometer system.

3   Roughness geometry and ranges

Two GI sheets of size 1200 mm × 330 mm × 1 mm have been used each for smooth and roughened absorber plates. A wire of 2 mm diameter has been used as the roughness element. The wires have been provided on the roughened absorber plate at its air flow-side in the form of a parallel arc to create turbulence in the flow passage. Figures 4a and 4b show pictorial views of roughened absorber plates having arc shaped wire roughness with apex-downstream and apex-up stream respectively.

The values/range of geometrical parameters of solar air heater duct, roughness parameters and experimental conditions, e.g., mass flow rate, wind velocity, insolation, etc. used during experimentation have been given in Tab. 1b.

Table 1a: Comparison of different roughness and operating parameters between present experimental work and Saini and Saini [13].

No.		Parameter	Values/Range		Units
			Saini and Saini [13]	Present Work	
1	Mode of experiment	–	Indoor	Actual outdoor	–
2	Roughness parameters	Relative roughness pitch (P/e)	10	8–15	–
		Relative roughness height (e/D)	0.0213–0.0422	0.0454	–
		Angle of attack (α)	0.3333–0.6666	45–75°	–
		Duct aspect ratio (W/H)	12	11	–
3	Operating parameters	Mass flow rate ($\dot{m}$)	Not reported	0.0100–0.0471	kg/s
		Reynolds number (Re)	2000–17000	2983–13955	–
4	Arrangement of roughness geometry (arc-shape)		Apex-downstream flow	Apex-upstream and Apex-downstream flow	

Table 1b: Details of present experimental setup and operating conditions.

| No.		Parameter	Values/Range	Units
1	Duct parameters	Entry length	650	mm
		Test section length (L)	1200	mm
		Exit length	300	mm
		Width (W)	330	mm
		Height (H)	30	mm
		Duct aspect ratio (W/H)	11	–
		Hydraulic diameter (D)	55	mm
		Glass cover thickness (L_g)	4	mm
		Glass wool insulation thickness (δ_i)	50	mm
		Distance between top glass cover and absorber plate (L_1)	30	mm
2	Roughness parameters	Roughness height (e)	2	mm
		Relative roughness pitch (P/e)	8, 10, 15	–
		Relative roughness height (e/D)	0.0454	–
		Angle of attack (α)	45°, 60°, 75°	–
3	Operating parameters	mass flow rate ($\dot{m}$)	0.0100–0.0471	kg/s
		Reynolds number (Re)	2983–13955	–
4	Experimental conditions	Solar insolation (I)	600–900	W/m^2
		Ambient temperature (T_a)	19.5–40.0	°C
		Wind velocity (V_w)	0.3–4.5	m/s

(a)

(b)
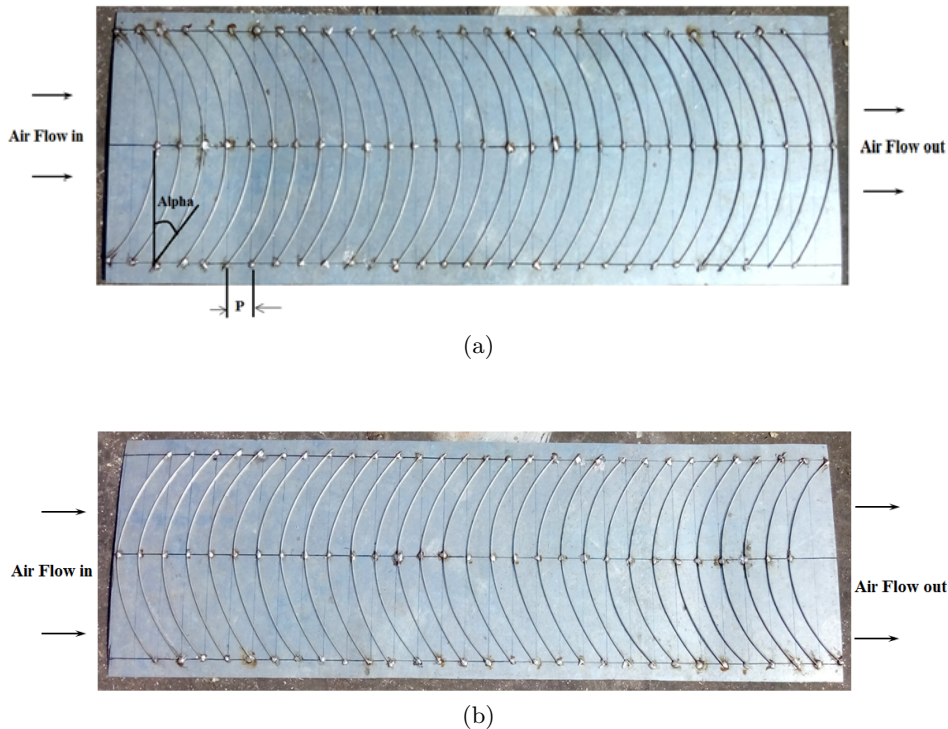
Figure 4: Photographic view of arc shape wire roughened absorber plate a) with apex-down stream flow, b) with apex-up stream flow.

3.1   Experimental procedure and data collection

Before starting the actual experiment, all the components of the setup and measuring instruments were checked for its proper operation. Before starting the experiment, the glass covers fitted on the heater test sections were properly cleaned. The control valves were kept closed before switching on the blower. The blower was switched on to ensure no leakage anywhere in the joints. The mass flow rate in the duct is adjusted using a control valve by observing the reading of U-tube manometer. Once the mass flow rate of air is fixed, all the readings are taken, when the system attains quasi-steady state, i.e., the temperatures do not change appreciably for at least 30 min of operation.

Test data were taken in outdoor condition in clear sky days between 10.30 to 14.30 hours at an interval of 30 min during the months of February to April, 2017.

The readings were recorded for all values of roughness parameters mentioned in Tab. 3 and six values of mass flow rate of air as mentioned in Tab. 2 in order to cover the entire range of Reynolds number (Re). A wide range of experimental data for 60 numbers of test runs with 6 different sets of roughened absorber plates and 1 smooth absorber plate was collected simultaneously.

Table 2: Values of mass flow rate ($\dot{m}$) and mass flow rate per unit area (G) of air used in the experimental investigation.

No.	Δh (mm of water column)	$\dot{m}$ (kg/s)	G (kg/s m^2)	Reynolds number Re
1	8	0.0100	0.0252	2983
2	20	0.0159	0.0401	4717
3	50	0.0252	0.0636	7459
4	80	0.0319	0.0805	9435
5	120	0.0390	0.0984	11556
6	175	0.0471	0.1189	13955

Details of 60 numbers of experimental test runs of roughened and smooth absorber plate SAHs have been given in Tab. 3.

Table 3: Details of experimental test runs conducted for roughened and smooth absorber plate SAHs (for $\dot{m} = 0.01$–0.047 kg/s).

No.	Run number	Arrangement of arc shaped wire roughness	Mass flow rate $\dot{m}$ (kg/s)	Relative roughness pitch, P/e	Relative roughness height, e/D	Angle of attack, α
1	1–6	Apex-downstream	0.01–0.047	10	0.0454	45°
2	7–12	Apex-upstream	0.01–0.047	10	0.0454	45°
3	13–18	Apex-downstream	0.01–0.047	10	0.0454	60°
4	19–24	Apex-upstream	0.01–0.047	10	0.0454	60°
5	25–30	Apex-downstream	0.01–0.047	10	0.0454	75°
6	31–36	Apex-upstream	0.01–0.047	10	0.0454	75°
7	37–42	Apex-downstream	0.01–0.047	8	0.0454	60°
8	43–48	Apex-upstream	0.01–0.047	8	0.0454	60°
9	49–54	Apex-downstream	0.01–0.047	15	0.0454	60°
10	55–60	Apex-upstream	0.01–0.047	15	0.0454	60°

The parameters measured (for both SAHs ducts) during experimentation are:

(a) pressure drop across orifice plate,

(b) inlet air temperature,

(c) outlet air temperature,

(d) temperature of absorber plate,

(e) pressure drop across the test section,

(f) solar radiation intensity,

(g) ambient temperature.

3.2   Data reduction

The experimental data, such as pressure drops across orifice plate and test section, inlet and outlet temperatures of air and temperatures of the absorber plate at various locations in the duct were recorded in clear sky days.

The mass flow rate has been calculated as follows:

$$\dot{m} = C_d A_o \sqrt{\frac{2\rho\,\Delta P_o}{1 - \beta_R^4}}\,, \tag{1}$$

where: C_d – coefficient of orifice discharge, A_o – area of orifice, ΔP_o – pressure drop across orifice meter and β_R – ratio of orifice diameter (D_2) to flow pipe internal diameter (D_1). In the present investigation the value of C_d has been taken as 0.60.

The pressure drop ΔP_o across the orifice meter has been calculated by using the manometric reading (Δh)

$$\Delta P_o = \rho g \Delta h \left(\frac{\rho_m}{\rho} - 1\right), \tag{2}$$

where: ρ_m – density of manometric fluid (water), g – gravitational acceleration.

For collector area (A_c) of 0.396 m^2 (1.2 m × 0.33 m) the value of mass flow rate per unit area of the collector (G) was computed. The values of mass flow rate $(\dot{m})$, and mass flow rate per unit collector area (G) have been listed in Tab. 2.

The heat gained by air and heat transfer coefficient have been calculated using the following equations:

$$Q_u = \dot{m}\, C_{pa}\, (T_{fo} - T_{fi})\,, \tag{3}$$

and

$$h = \frac{Q_u}{A_c(T_{pm} - T_{fm})}\,, \tag{4}$$

where A_c is the heat transfer area (area of absorber plate), T_{fm} and T_{pm} are average values of air and absorber plate temperatures, respectively

$$T_{pm} = \frac{T_1 + T_2 + T_3 + T_4 + \ldots + T_{15}}{15}\,, \tag{5}$$

$$T_{fm} = \frac{T_{fi} + T_{fo}}{2}\,. \tag{6}$$

3.3 Representation of thermal performance and evaluation of performance parameters

As discussed in earlier, the thermal efficiency of a solar air heater drawing air at ambient temperature $(T_{fi} = T_a)$ can be expressed as

$$\eta_{th} = F_o \left[(\tau\alpha_p)_e - U_L \frac{(T_{fo} - T_{fi})}{I} \right]. \tag{7}$$

The thermal efficiency can also be expressed by another equation in terms of temperature rise of working fluid as

$$\eta_{th} = GC_{pa} \frac{(T_{fo} - T_{fi})}{I} = GC_{pa} \frac{\Delta T}{I}\,. \tag{8}$$

Thus, a single plot with efficiency η_{th}, as ordinate and temperature rise parameter $(\Delta T/I)$, as abscissa can be used to represent Eqs. (7) and (8). This is considered to be the most appropriate representation of the thermal performance of such solar air heaters. In order to obtain complete information with regard to the thermal performance of solar air heaters, it therefore becomes necessary to conduct tests over a wide range of mass flow rate with each flow rate yielding its own efficiency curve [22, 23]. For solar air heaters that sucks air directly from the atmosphere $(T_{fi} = T_a)$, Eq. (7) becomes irrelevant, since abscissa is always zero, if $T_{fi} = T_a$. Therefore, to obtain complete design information for such systems, a single performance

plot (η_{th} versus $\Delta T/I$) representing Eqs. (7) and (8) for different mass flow rates can be drawn.

In view of the above, performance plots for arc-shaped apex-upstream and apex-downstream and also for plane solar air heaters have been prepared by using experimental data.

A sample plot as shown in Fig. 7 represents a plot of efficiency against the temperature rise parameter $(T_{fo}-T_{fi})/I$ using Eq. (7) which represents the best fit lines of the efficiency data points for various operating parameters at a given set of system parameters for arc shaped roughened and smooth plate SAH and using Eq. (8) which shows the plot of efficiency for given mass flow rate and for a given values of roughness parameters.

3.4 Evaluation of overall loss coefficient, collector heat removal factor and collector efficiency factor

The overall loss coefficient (U_L), for the collector can be evaluated using the values of the parameters $F_o(\tau\alpha_p)_e$ and F_oU_L obtained from the corresponding performance plot and with the use of suitable value of the effective absorptance-transmittance product $(\tau\alpha_p)_e$ for the collector.

Using experimental values of parameter $F_o(\tau\alpha_p)_e$ and F_oU_L from the thermal performance characteristics curves the values of performance parameters F_R and F' for a given mass flow rate of air can be obtained from [18, 23]

$$F_R(\tau\alpha_p)_e = F_o(\tau\alpha_p)_e \left[\frac{GC_{pa}}{GC_{pa} + F_oU_L} \right], \tag{9}$$

$$F_RU_L = F_oU_L \left[\frac{GC_{pa}}{GC_{pa} + F_oU_L} \right]. \tag{10}$$

The collector efficiency factor (F'), at a given mass flow rate of air can be evaluated using the corresponding values of collector heat removal factor (F_R), and overall loss coefficient (U_L)

$$F'U_L = -GC_{pa} \ln \left[1 - \frac{F_RU_L}{GC_{pa}} \right]. \tag{11}$$

3.5 Test for validation

The Nusselt number (Nu) and friction factor (f) for the collector test sections were calculated by using the following relationships:

$$\text{Nu} = \left[\frac{hD}{K_a}\right],$$ (12)

$$D = \frac{2WH}{(W+H)},$$ (13)

$$f = \frac{2\rho(\Delta P_D)D}{4L_f \dot{M}^2},$$ (14)

where: ΔP_D – pressure drop across the duct, L_f – the distance between two pressure taps in the duct, $\dot{M} = \left(\dfrac{\dot{m}}{WH}\right)$ – mass velocity of air.

The Reynolds number is

$$\text{Re} = \frac{\dot{M}D}{\mu}.$$ (15)

To validate experimental data, the experimental values of Nusselt number and friction factor for smooth duct were computed and compared with the values obtained by using Dittus–Boelter equation [24] and modified Blasius equation [25, 33] for Nusselt number and friction factor, given respectively as:

$$\text{Nu}_s = 0.024\,\text{Re}^{0.8}\text{Pr}^{0.4},$$ (16)

$$f_s = 0.085\,\text{Re}^{-0.25}.$$ (17)

The experimental values and predicted values of Nusselt number and friction factor as a function of Reynolds number have been plotted in Figs. 5a and 5b respectively, for smooth absorber plate SAH.

The experimental values of Nusselt number have been compared to that obtained by using Dittus–Boelter equation, which shows a very little deviation of $\pm 2.3\%$.

Similarly, in the plot of friction factor versus Reynolds number in Fig. 5b for experimental and predicted values, shows a very small deviation. Thus, a reasonably good agreement between the experimental and predicted results is obtained, which ensures the accuracy of the data collected.
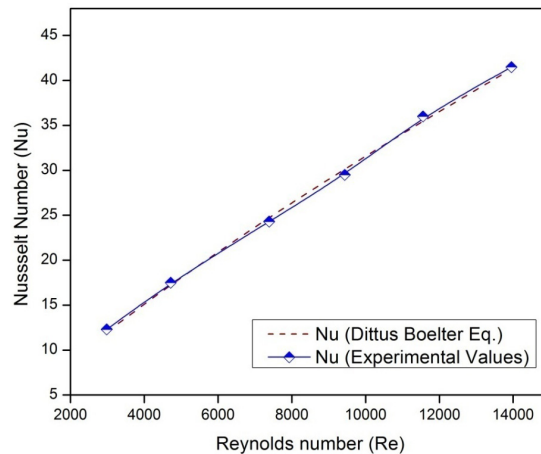
(a)
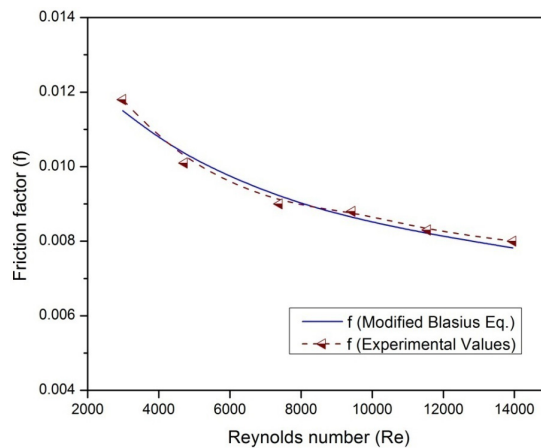
(b)

Figure 5: Comparison of experimental values and predicted values: a) of Nusselt number for smooth absorber plate duct, b) of Friction factor for smooth absorber plate duct.

4   Results and discussion

The results obtained from experimentation on the thermal performance of apex-upstream and apex-downstream flow roughened SAHs have been presented and discussed. The performance characteristics of these heaters have been compared with the smooth absorber plate solar air heater under similar geometrical and operating conditions.

The effect of roughness parameters, i.e., relative roughness pitch and angle of attack on the thermal performance, collector heat removal factor, collector efficiency factor and pressure drop has been discussed.

4.1   Thermal performance of collector

Figures 6 to 11 shows the plots of experimental values of thermal efficiencies as a function of temperature rise parameter ($\Delta T/I$) of arc-shaped apex-upstream, apex-downstream roughened and plane absorber plate SAHs for various values of relative roughness pitch (P/e) and constant values of $e/D = 0.0454$ and $\alpha = 60°$. Each line of these figures has been obtained from the linear regression fit of the data for the corresponding P/e for roughened and plane SAHs.

The values of thermal efficiencies for apex-upstream, apex-downstream and smooth absorber plate SAHs at the two extreme mass flow rates in terms of Reynolds number (Re = 2983 and 13955) obtained from the corresponding regression lines have been listed in Tab. 4. The corresponding enhancement has also been given in this table.

4.1.1   Effect of relative roughness pitch

Figure 6 shows the thermal efficiency as a function of temperature rise parameter ($\Delta T/I$) with different mass flow rates for arc-shaped wire rough-
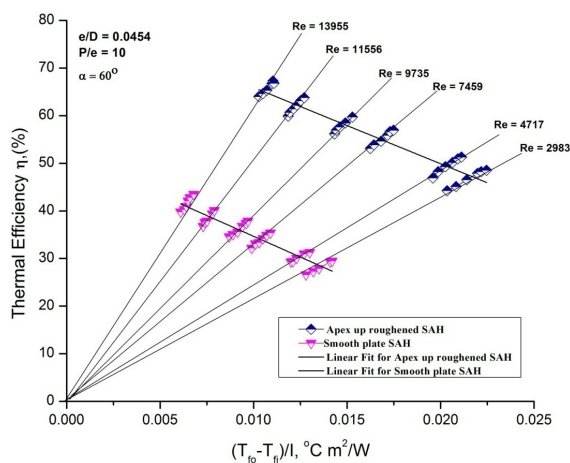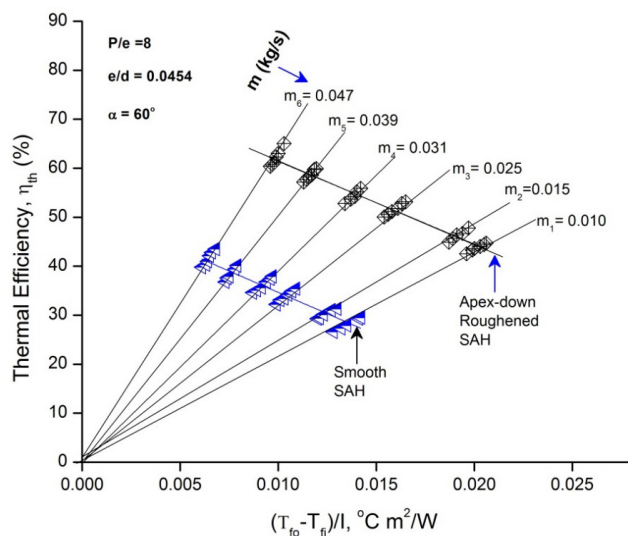

Figure 6: Thermal performance plot of arc-shaped wire roughened with apex-upstream SAH with $P/e = 10$, $e/D = 0.0454$, and $\alpha = 60°$.

ness with apex-upstream SAH, for $P/e = 10$, $e/D = 0.0454$, and $\alpha = 60°$. It can be seen from Fig. 6 that the thermal efficiency of a smooth absorber plate solar air heater increases from 27.2% to 41.2% as Reynolds number increases from Re $= 2983$ ($\dot{m} = 0.010$ kg/s) to Re $= 13955$ ($\dot{m} = 0.047$ kg/s). The corresponding value of thermal efficiency for Apex-Upstream roughened SAH has been obtained as 46.7% to 69.2%. For mass flow rate of 0.010 to 0.047 kg/s (Re $= 2983$ to 13955), the regression fit line shows an enhancement in thermal efficiency in the range of 44.3–71.6% as compared to plane SAH, which has also been tabulated in Tab. 4.

Figures 7 and 9 shows the effect of relative roughness pitch on the thermal efficiency of arc-shaped wire roughened with apex-upstream and apex-downstream SAHs respectively as a function of temperature rise parameter ($\Delta T/I$). The curves show that the thermal efficiency of solar air heater increases appreciably with the use of artificial roughness on the absorber plates.
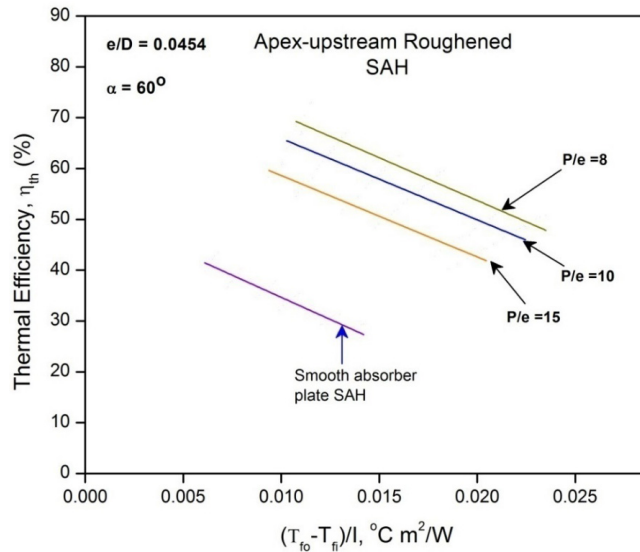
Figure 7: Thermal performance plot of arc-shaped wire roughened with apex-upstream SAH for different P/e.

It can also be seen from Figs. 6 to 9 and Tab. 4 that the thermal efficiency of both roughened SAHs decreases with an increase in relative roughness pitch for fixed values of e/D and α. It is observed that for both roughened SAHs thermal efficiency is maximum corresponding to the relative rough-

Table 4: Collector thermal efficiencies of apex-upstream, apex-downstream roughened and smooth plate SAHs and their corresponding enhancement for different relative roughness pitch, based on regression linear fit lines.

e/D	α	P/e	Reynolds number, Re	Efficiency of apex-upstream roughened SAH (%)	Efficiency of apex-downstream roughened SAH (%)	Efficiency of smooth plate SAH (%)	Enhancement in η_{th} for apex-upstream (%)	Enhancement in η_{th} for apex-downstream (%)
0.0454	60°	8	2983	46.7	42.4	27.2	**71.6**	**55.8**
			13955	69.2	61.9	41.2	67.9	50.2
0.0454	60°	10	2983	45.8	41.4	28.4	61.2	45.7
			13955	65.2	59.1	40.8	59.8	44.8
0.0454	60°	15	2983	41.5	37.6	27.4	51.4	37.2
			13955	59.6	53.8	41.3	44.3	30.3

Figure 8: Thermal performance plot of arc-shaped wire roughened with apex-downstream SAH with $e/D = 0.0454$, $P/e = 8$, and $\alpha = 60°$.
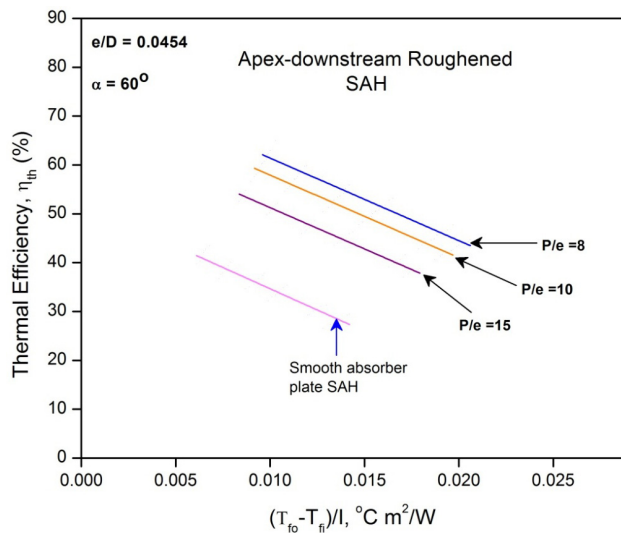
Figure 9: Thermal performance plot of arc-shaped wire roughened with apex-downstream SAH for different P/e.

ness pitch $P/e = 8$ and thermal efficiency decreases with increasing P/e from 8. It is due to the fact that flow separation occurs downstream of an

attached rib and the reattachment of the free shear layer may not occur if
P/e value is less than 8 and maximum heat transfer always occurs in the
vicinity of reattachment point and if the value of P/e is more than 8 then
the formation in the number of reattachment points decreases as the gap
between the roughness element increases which results in less heat transfer.
This result agrees with the result of Varun *et al.* [26], Aharwal *et al.* [27],
Hans *et al.* [5], and Singh *et al.* [28].

Arc-shaped wire with apex-upstream SAH is having higher value of ther-
mal efficiency because there is more dispersion of flow in this case as com-
pared to arc-shaped wire with apex-downstream flow, which causes more
turbulence in the flow.

4.1.2 Effect of angle of attack

Figures 10 and 11 show the effect of different values of angle of attack (α)
on thermal performance of apex-upstream and apex-downstream roughened
SAHs respectively as a function of temperature rise parameter ($\Delta T/I$).
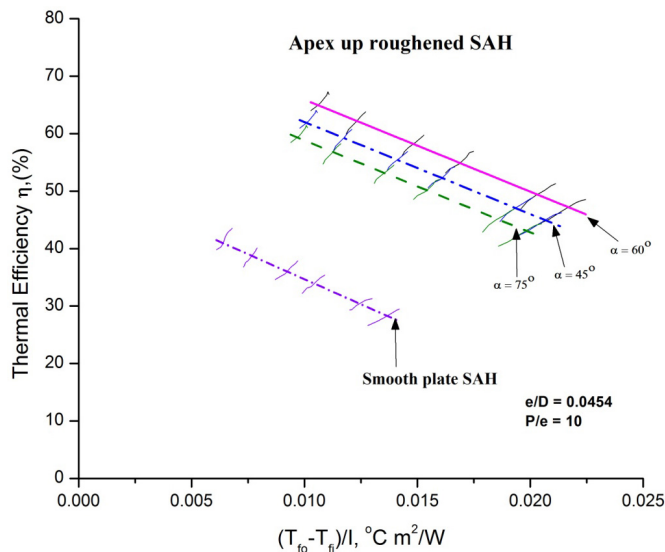
Figure 10: Thermal performance plot of apex-upstream roughened SAH for different an-
gle of attack.

It has been observed from these figures and Tab. 5, that for both roughened
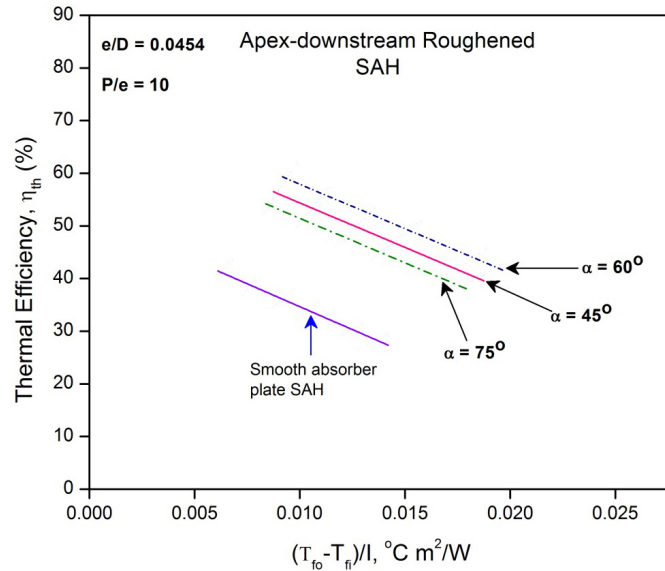SAHs thermal efficiency is maximum corresponding to angle of attack $\alpha =$

Figure 11: Thermal performance plot of Apex-Downstream roughened SAH for different angle of attack.

$60°$ and thermal efficiency having lower values for other values of angle of attack (i.e., $\alpha = 45°$ and $\alpha = 75°$) as compared to $\alpha = 60°$. The strength of secondary flow across the rib roughness changes with change in angle of attack. This variation in heat transfer, thereby, the thermal efficiency is caused by interaction of secondary-flow along the rib and boundary layer on flow upstream side of the wire rib. The boundary layer is due to main flow with the roughened surface and originates from the flow reattachment point between the ribs up to the succeeding downstream rib.

The possible reason for attaining thermal efficiency, maximum at the value corresponding to $\alpha = 60°$ is that the separation of secondary flow due to the presence of roughness elements (at this value of inclination) and the movement of vortices combining together, maximum occurs at this value of angle of attack. This result agrees with the result of Momin *et al.* [4], Aharwal *et al.* [27], Lanjewar *et al.* [8], and Singh *et al.* [29].

Another important point worth-noting that emerges from the result of Figs. 6–13 is the linear relationship between thermal efficiency and temperature rise parameter at a given mass flow rate exists.

M.K. Sahu, M.M. Matheswaran and P. Bishnoi

Table 5: Collector thermal efficiencies of apex-upstream, apex-downstream roughened and smooth plate SAHs and their corresponding enhancement for different angle of attack, based on regression linear fit lines.

e/D	α	P/e	Reynolds number, Re	Efficiency of apex-upstream roughened SAH (%)	Efficiency of apex-downstream roughened SAH (%)	Efficiency of smooth plate SAH (%)	Enhancement in η_{th} for apex-upstream (%)	Enhancement in η_{th} for apex-downstream (%)
0.0454	10	45°	2983	43.4	39.2	27.4	58.4	43.0
			13955	62.5	56.5	41.2	51.6	37.2
0.0454	10	60°	2983	45.8	41.4	27.4	**67.1**	**51.0**
			13955	65.2	59.1	41.2	58.2	43.4
0.0454	10	75°	2983	41.7	37.2	27.4	52.1	35.4
			13955	59.8	54.4	41.2	45.1	32.0

4.2 Collector heat removal factor and collector efficiency factor

4.2.1 Effect of relative roughness pitch

The values of parameters $F_o(\tau\alpha_p)_e$ and F_oU_L obtained from the intercept and slope respectively of the performance curves obtained from the experimental results have already been given in Tab. 6 for the three collectors. The values of performance parameters; the heat removal factor and collector efficiency factor, were plotted for different values of P/e and α as a function of mass flow rates for all three collectors in Figs. 12 to 16.

Figure 12 shows the comparison of heat removal factor and collector efficiency factor for both roughened and smooth plate SAHs. The fixed
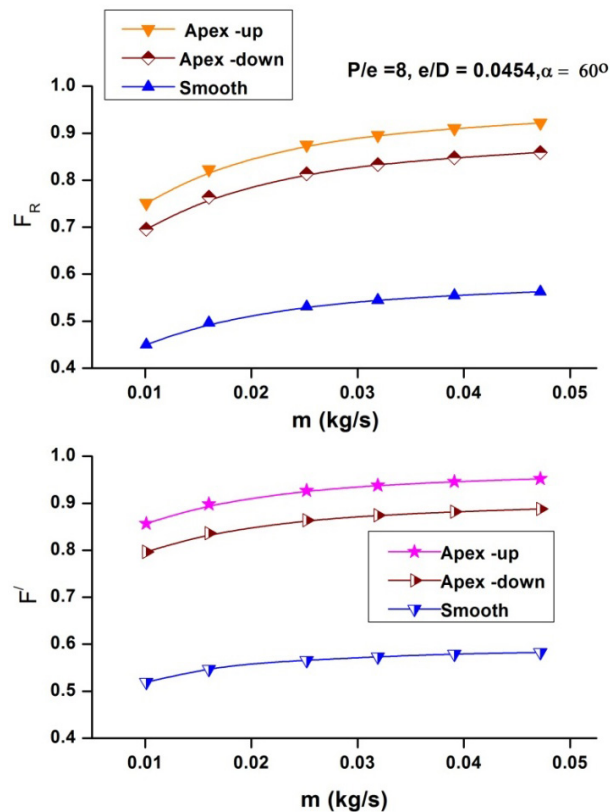
Figure 12: Plots of heat removal factor and collector efficiency factor as a function of mass flow rate for all three collectors.

roughness parameters were taken as $e/D = 0.0454$, $P/e = 8$, and $\alpha = 60°$. It can be observed that F_R and F' increase with mass flow rates in general. The values of F_R and F' are higher for apex-upstream flow SAH as compared to those for apex downstream and plane SAHs.

Figures 13 and 14 show the effect of different P/e and comparison on the collector heat removal factor and collector efficiency factor for apex-upstream and apex-downstream roughened SAHs, respectively. It can be seen from these figures that both F_R and F' have been found to increase with a decrease in the values of P/e from 15 to 8 and increasing the mass flow rate for fixed values of roughness parameters as $e/D = 0.0454$ and $\alpha = 60°$.
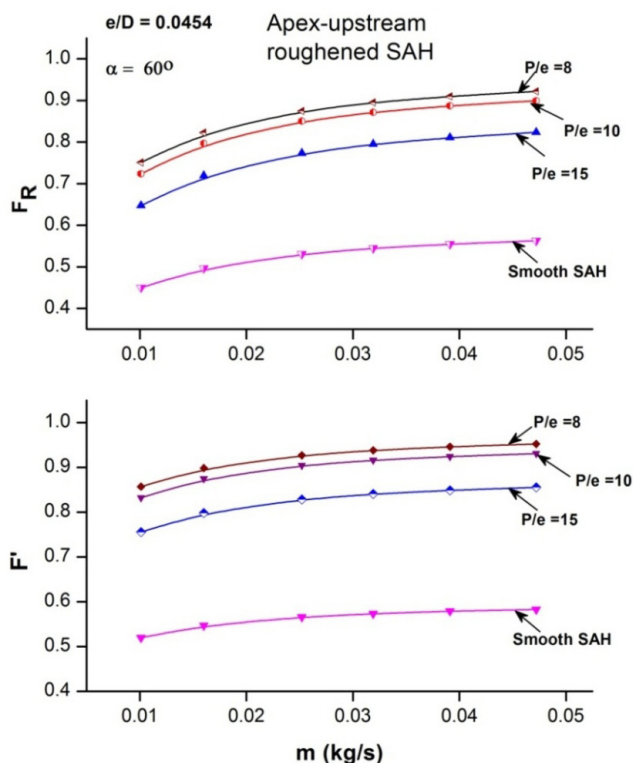
Figure 13: Effect of P/e on heat removal factor (F_R) and collector efficiency factor (F') for apex-upstream and smooth plate SAHs.

In this range, the heat removal factor for apex-upstream roughened collector has been found to be higher by a factor of 1.67, 1.60 and 1.46 with respect to a smooth plate SAH for P/e of 8, 10 and 15, respectively.
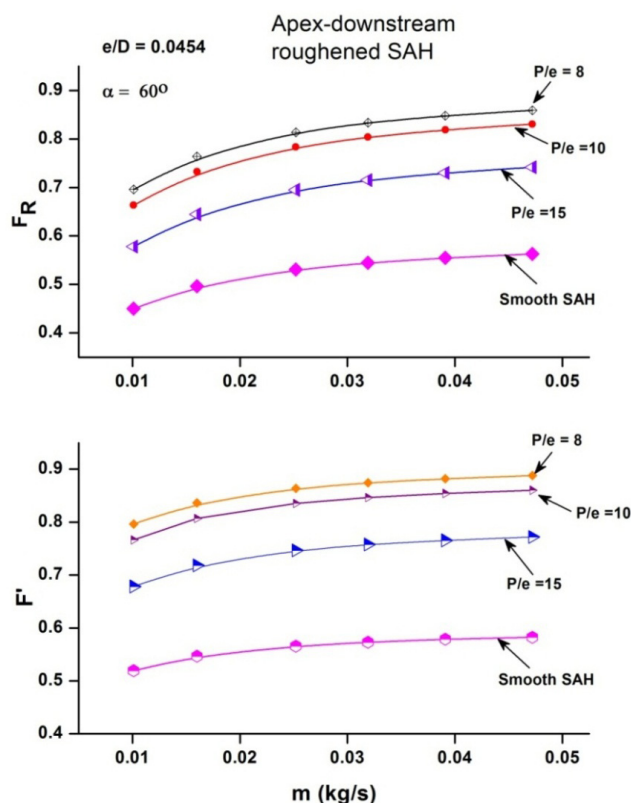
Figure 14: Effect of P/e on heat removal factor (F_R) and collector efficiency factor (F') for apex-downstream and smooth plate SAHs.

Furthermore, for apex-down roughened SAH, F_R is higher by a factor of 1.54, 1.47 and 1.31 as compared to smooth SAH for relative roughness pitch of 8, 10 and 15 respectively.

4.2.2 Effect of angle of attack

Figures 15 and 16 show the effect of different values of angle of attack and comparison of heat removal factor and collector efficiency factor for both roughened and smooth plate SAHs. It can be observed that F_R and F' increase with mass flow rates in general. The values of F_R and F' for apex-upstream is higher as compared to apex downstream and smooth absorber plate SAHs. Furthermore, it can also be concluded from these figures that for both roughened SAHs, F_R and F' are maximum corresponding to $\alpha =$

$60°$ among the three values of angle of attack ($\alpha = 45°$, $60°$, and $75°$) used in the present investigation.
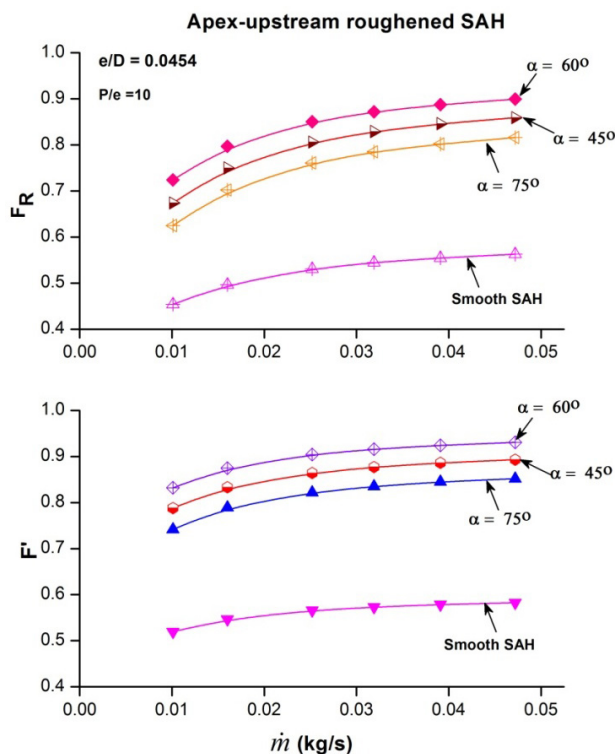

Figure 15: Effect of angle of attack (α) on heat removal factor (F_R) and collector efficiency factor (F') for apex-upstream and smooth plate SAHs.

Figure 17 shows the thermal efficiency comparison of present apex-upstream SAH with $P/e = 8$, $e/D = 0.0454$ and $\alpha = 60°$ with some other artificial roughened and smooth plate SAHs efficiencies which have been analyzed on actual outdoor experimental conditions and reported in the literature. The thermal efficiency of present SAH is greater than 1-sided transverse wire SAH used by Prasad [31, 32] and 1-sided transverse wire SAH used by Behura *et al.* [23]. It can also be seen from the figure that present SAH have higher thermal efficiency over 3-sided transverse wire SAH used by [23] for ($\Delta T/I > 0.010$).

This may because in 3-sided SAH, the wires in the 3 sides of the plates enhances the heat transfer area as well as heat transfer coefficient more than the 1-sided rough and the smooth SAH. Furthermore present results holds
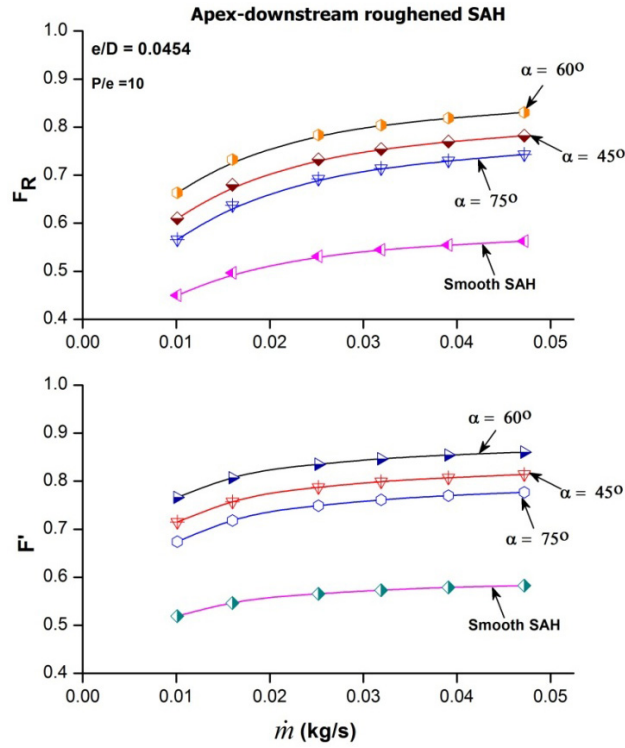
Figure 16: Effect of angle of attack (α) on heat removal factor (F_R) and collector efficiency factor (F') for apex-downstream and smooth plate SAHs.
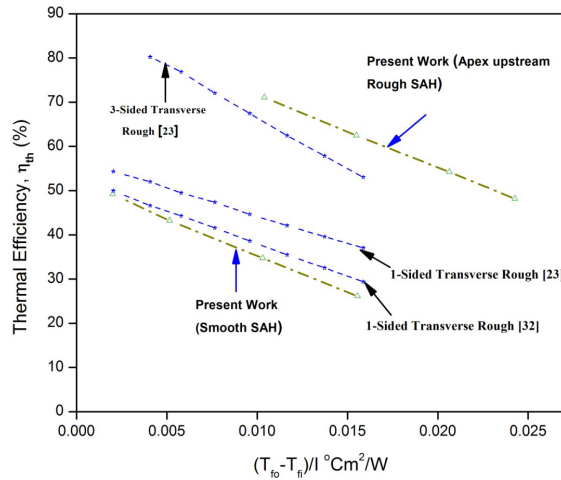

Figure 17: Thermal efficiency comparison of present apex-upstream SAH as function of temperature rise parameters ($\Delta T/I$) with some SAHs available in the literature.

a good agreement between the previous experimental values and makes the perfection of present data collected through experimentation.

5   Conclusions

Based on the experimental results of the arc shaped wire roughened for apex-upstream and apex-downstream geometries, the following main conclusions were drawn

1. Thermal efficiency of the roughened and simple smooth plate SAHs increases with the increasing values of mass flow rate and decreases with an increase in the relative roughness pitch (P/e) for fixed values of relative roughness height (e/D) and angle of attack (α).

2. Apex-upstream roughened SAH is having higher value of thermal efficiency, collector heat removal factor (F_R) and collector efficiency factor (F') as compared to apex-downstream roughened and simple smooth plate SAHs.

3. For the range of mass flow rate from 0.010 kg/s to 0.047 kg/s, both the apex-upstream and downstream configurations designs, the relative roughness pith $P/e = 8$ and angle of attack $\alpha = 60°$ yields the maximum thermal efficiency of 69.2% and 61.9% respectively.

4. Maximum enhancement in thermal efficiency has been found to be 71.6% for apex-upstream whereas for apex-downstream SAH it was obtained as 55.8% as compared to the simple plane SAH with the range, values of geometric, roughness and operating parameters which have been used for present analysis.

References

[1] Prasad B.N., Saini J.S.: *Effect of artificial roughness on heat transfer and friction factor in a solar air heater.* Sol. Energy **41**(1988), 555–560.

[2] Gupta D., Solanki S.C., Saini J.S.: *Thermohydraulic performance of solar air heaters with roughened absorber plates.* Sol. Energy **61**(1997), 33–42.

[3] Aharwal K.R., Gandhi B.K., Saini J.S.: *Experimental investigation on heat-transfer enhancement due to a gap in an inclined continuous rib arrangement in a rectangular duct of solar air heater.* Renew. Energ. **33**(2008), 585–596.

[4] Momin A.-M.E., Saini J.S., Solanki S.C.: *Heat transfer and friction in solar air heater duct with v-shaped rib roughness on absorber plate.* Int. J. Heat Mass Tran. **45**(2002), 16, 3383–3396.

[5] Hans V.S, Saini R.P., Saini J.S.: *Heat transfer and friction factor correlations for a solar air heater duct roughened artificially with multiple V-ribs.* Sol. Energy **84**(2010), 898–911.

[6] Kumar A., Saini R.P., Saini J.S.: *Development of correlations for Nusselt number and friction factor for solar air heater with roughened duct having multi v-shaped with gap rib as artificial roughness.* Renew. Energ. **58**(2013), 151–163.

[7] Kumar A., Bhagoria J.L., Sarviya R.M.: *Heat transfer enhancement in channel of solar air collector by using discrete w-shaped artificial roughened absorber.* In: Proc. 19th National and 8th ISHMT-ASME Heat and Mass Transfer Conf. (2009).

[8] Lanjewar A., Bhagoria J.L., Sarviya R.M.: *Experimental study of augmented heat transfer and friction in solar air heater with different orientations of W-Rib roughness.* Exp. Thermal Fluid Sci. **35**(2011), 986–995.

[9] Singh A.P., Varun, Siddhartha: *Effect of artificial roughness on heat transfer and friction characteristics having multiple arc shaped roughness element on the absorber plate.* Sol. Energy **105**(2014), 479–493.

[10] Pandey N.K., Bajpai V.K., Varun: *Experimental investigation of heat transfer augmentation using multiple arcs with gap on absorber plate of solar air heater.* Sol. Energy **134**(2016), 314–26.

[11] Hans V.S., Gill R.S., Singh S.: *Heat transfer and friction factor correlations for a solar air heater duct roughened artificially with broken arc ribs.* Exp. Therm. Fluid Sci. **80**(2017), 77–89.

[12] Gill R.S., Hans V.S., Saini J.S., Singh S.: *Investigation on performance enhancement due to staggered piece in a broken arc rib roughened solar air heater duct.* Renew. Energ. **104**(2017), 148–162.

[13] Saini S.K., Saini R.P.: *Development of correlations for Nusselt number and friction factor for solar air heater with roughened duct having arc-shaped wire as artificial roughness.* Sol. Energy **82**(2008), 1118–1130.

[14] Sahu M.K., Prasad R.K.: *Investigation on optimal thermohydraulic performance of a solar air heater having arc shaped wire rib roughness on absorber plate.* Int. J. Thermodyn. **19**(2016), 214–224.

[15] Sahu M.K., Prasad R.K.: *Exergy based performance evaluation of solar air heater with arc-shaped wire roughened absorber plate.* Renew. Energ. **96**(2016), 233–243.

[16] Sahu M.K., Prasad R.K.: *Thermohydraulic performance analysis of an arc shape wire roughened solar air heater.* Renew. Energ. **108**(2017), 598–614.

[17] Sahu M.K., Prasad R.K.: *Entropy generation and thermodynamic analysis of solar air heaters with artificial roughness on absorber plate.* Arch. Thermodyn. **38(**2017), 3, 23–48.

[18] Prasad R.K.: *Thermal performance characteristics of unidirectional flow porous bed solar energy collectors for heating air.* PhD thesis, IIT, Roorkee 1993.

[19] Sahu M.K., Prasad R.K.: *A review of the thermal and hydrodynamic performance of solar air heater with roughened absorber plates.* J. Enhanc. Heat Transf. **23**(2016), 1, 47–89.

[20] Sahu M.K.: *Thermohydraulic Performance of Solar Air Heater with Arc-Shaped Wire Roughened Absorber Plates.* PhD thesis, NIT, Jamshedpur 2017.

[21] ASHRAE standard 93–97: *Method of testing to determine the thermal performance of solar collector*, 1977.

[22] Biondi P., Cicala F.L., Farina, G.: *Performance analysis of solar air heaters of conventional design.* Sol. Energy **41**(1988), 1, 101–107.

[23] Behura Arun K., Prasad B.N., Prasad L.: *Heat transfer, friction factor and thermal performance of three sides artificially roughened solar air heaters.* Sol. Energy **130** (2016), 46–59.

[24] Rohsenow W.M., Hartnett J.P., Cho Y.I. (Eds.): *Handbook of Heat Transfer.* McGraw Hill, New York 1998.

[25] Bhatti M.S., Shah R.K.: *Turbulent flow convective heat transfer.* In: S. Kakac, R.K. Sash, W. Aung (Eds.): Handbook of single phase convective heat transfer. John Willey & Sons, New York 1987.

[26] Varun, Patnaik A., Saini R.P, Singal S.K, Siddhartha: *Performance prediction of solar air heater having roughened duct provided with transverse and inclined ribs as artificial roughness.* Renew. Energ. **34**(2009), 2914–2922.

[27] Aharwal K.R., Gandhi B.K., Saini J.S.: *Heat transfer and friction characteristics of solar air heater ducts having integral inclined discrete ribs on absorber plate.* Int. J. Heat Mass Tran. **52**(2009), 5970–5977.

[28] Singh S., Chander S., Saini J.S.: *Exergy based analysis of solar air heater having discrete V-down rib roughness on absorber plate.* Energy **37**(2012), 749–758.

[29] Singh S., Chander S., Saini J.S.: *Thermal and effective efficiency based analysis of discrete V-down rib-roughened solar air heaters.* J. Renew. Sustain. Ener. **3**(2011), 023107.

[30] Kline S.J., McClintock F.A.: *Describing uncertainties in single sample experiments.* Mech. Eng. **75**(1953), 3–8.

[31] Prasad B.N.: *Thermal performance of artificially roughened solar air heaters.* Sol. Energy **91**(2013), 59–67.

[32] Sahu M.K., Prasad R.K.: *Second law optimization and parametric study of a solar air heater having artificially roughened absorber plate.* Arch. Thermodyn. **40**(2019), 2, 107–135.

[33] Sahu M.K., Sharma M., Matheswaran M.M., Maitra K.: *On the use of longitudinal fins to enhance the performance in rectangular duct of solar air heaters – a review.* J. Sol. Energy Eng. **141**(2019), 1–16.

APPENDIX-A

UNCERTAINTY ANALYSIS

A methodology of estimating the uncertainty in experimental results has been suggested by Kline and Mc Clintock, which is used in this work. The procedure is listed as below [30]:

The uncertainty analysis as proposed [30] was used to calculate the uncertainty associated with experimental results, based on the observations in the measured values used in calculating the result.

If a parameter is calculated using certain measured quantities as,

$$Y = y(x_1, x_2, x_3, \ldots, x_n),$$

then uncertainty in the measurement of 'y' is given as follows:

$$\frac{\delta y}{y} = \left[\left(\frac{\partial y}{\partial x_1} \delta x_1 \right)^2 + \left(\frac{\partial y}{\partial x_2} \delta x_2 \right)^2 + \left(\frac{\partial y}{\partial x_3} \delta x_3 \right)^2 + \ldots + \left(\frac{\partial y}{\partial x_n} \delta x_n \right)^2 \right]^{0.5}.$$

Table A1: Error for different measurements.

No.	Measurement and symbol	Instrument	Least count	Error
1	Length, L	Linear scale	1 mm	± 1 mm
2	Duct height, H	Vernier scale	0.05 mm	± 0.05 mm
3	Duct width, W	Linear scale	0.05 mm	± 0.05 mm
4	Diameter of orifice meter, D_2	Vernier scale	0.05 mm	± 0.05 mm
5	Atmospheric pressure, P_{atm}	Mercury barometer	0.1 mm	± 0.1mm
6	Temperature measurement	Digital thermometer		$\pm 0.25°$C
7	Pressure drop across orifice meter (ΔP_o)	U-tube manometer	1 mm of water	± 1 mm
8	Insolation (I)	Pyranometer	1 W/m^2	± 1 W/m^2

(1) Hydraulic diameter of duct (D)

$$D = \frac{2WH}{(W + H)},$$

$$\frac{\delta D}{D} = \left[\left(\frac{\delta A}{A}\right)^2 + \left(\frac{\delta P}{P}\right)^2\right]^{0.5}$$
$$= \left[(1.67 \cdot 10^{-3})^2 + (3.34 \cdot 10^{-3})^2\right]^{0.5}$$
$$= 3.73 \cdot 10^{-3} \quad \text{or} \quad 0.003740.$$

(2) Area of orifice meter (A_o)

$$A_o = \frac{\pi}{4}D_2^2 \,,$$
$$\frac{\delta A_o}{A_o} = \left[\frac{2\,\delta D_2}{D_2}\right],$$
$$\frac{\delta A_o}{A_o} = \left[\frac{2 \cdot (0.05)}{38}\right]$$
$$= 2.631 \cdot 10^{-3} \quad \text{or} \quad 0.002631.$$

(3) Density (ρ)

$$\rho = \frac{P_{atm}}{R \cdot T_{fo}} \,,$$
$$\frac{\delta \rho}{\rho} = \left[\left(\frac{\delta P_{atm}}{P_{atm}}\right)^2 + \left(\frac{\delta T_o}{T_o}\right)^2\right]^{0.5},$$
$$\frac{\delta \rho}{\rho} = \left[\left(\frac{0.1}{99}\right)^2 + \left(\frac{0.25}{38.03}\right)^2\right]^{0.5}$$
$$= 6.6509 \cdot 10^{-3} \quad \text{or} \quad 0.006650.$$

(4) Mass flow rate $(\dot{m})$

$$m = C_d A_o \sqrt{\frac{2\rho(\Delta P_o)}{1 - \beta_R^4}} \,,$$
$$\frac{\delta m}{m} = \left[\left(\frac{\delta C_d}{C_d}\right)^2 + \left(\frac{\delta A_o}{A_o}\right)^2 + \left(2\frac{\delta \rho}{\rho}\right)^2 + \left(\frac{\delta(\Delta P_o)}{(\Delta P_o)}\right)^2 \left(\frac{2 \cdot \beta_R^3 \cdot \delta\beta_R}{1 - \beta_R^2}\right)\right]^{0.5},$$

$$\frac{\delta m}{m} = \left[\left(\frac{0.005}{0.60}\right)^2 + (0.002631)^2 + (2 \cdot 0.006650)^2\right.$$

$$\left. + \left(\frac{0.5}{490.5}\right)^2 \left(\frac{2 \cdot (0.6)^{0.3} \cdot (0.0015)}{1 - 0.6^4}\right)\right]^{0.5}$$

$$= 0.0315 \quad \text{or} \quad 3.157\%.$$

(5) Velocity of air test section (V)

$$V = \frac{\dot{m}}{\rho \cdot (WH)},$$

$$\frac{\delta V}{V} = \left[\left(\frac{\delta m}{m}\right)^2 + \left(\frac{\delta \rho}{\rho}\right)^2 + \left(\frac{\delta W}{W}\right)^2 + \left(\frac{\delta H}{H}\right)^2\right]^{0.5},$$

$$\frac{\delta V}{V} = \left[(0.00876)^2 + (0.00650)^2 + \left(\frac{0.05}{330}\right)^2 + \left(\frac{0.05}{30}\right)^2\right]^{0.5}$$

$$= 0.01997 \quad \text{or} \quad 1.99\%.$$

(6) Reynolds number (Re)

$$\mathrm{Re} = \frac{\rho V D}{\mu},$$

$$\frac{\delta \mathrm{Re}}{\mathrm{Re}} = \left[\left(\frac{\delta V}{V}\right)^2 + \left(\frac{\delta \rho}{\rho}\right)^2 + \left(\frac{\delta D}{D}\right)^2 + \left(\frac{\delta \mu}{\mu}\right)^2\right]^{0.5},$$

$$\frac{\delta \mathrm{Re}}{\mathrm{Re}} = \left[(0.01997)^2 + (0.00650)^2 + (0.0166)^2 + \left(\frac{0.001}{1.87}\right)^2\right]^{0.5}$$

$$= 0.0210 \quad \text{or} \quad 2.10\%.$$

(7) Useful heat gain (Qu)

$$Qu = \dot{m} C_{pa} \cdot \Delta T,$$

$$\frac{\delta Qu}{Qu} = \left[\left(\frac{\delta m}{m}\right)^2 + \left(\frac{\delta C_{pa}}{C_{pa}}\right)^2 + \left(\frac{\delta(\Delta T)}{\Delta T}\right)^2\right]^{0.5},$$

$$\frac{\delta Qu}{Qu} = \left[(0.0315)^2 + \left(\frac{1.0}{1008} \right)^2 + \left(\frac{0.25}{7.7} \right)^2 \right]^{0.5}$$

$$= 0.0452 \quad \text{or} \quad 4.52\%.$$

(8) Thermal efficiency (η_{th})

$$\eta_{th} = \frac{Q_u}{I A_c},$$

$$\frac{\delta \eta_{th}}{\eta_{th}} = \left[\left(\frac{\delta Q_u}{Q_u} \right)^2 + \left(\frac{\delta I}{I} \right)^2 + \left(\frac{\delta(\Delta A_c)}{\Delta A_c} \right)^2 \right]^{0.5},$$

$$\frac{\delta \eta_{th}}{\eta_{th}} = \left[(0.0452)^2 + \left(\frac{1}{882} \right)^2 + (0.0008469)^2 \right]^{0.5}$$

$$= 0.046 \quad \text{or} \quad 4.6\%.$$